Analysis and experiment on cutting performances of high-stubble maize stalks

Zhao Jiale, Huang Dongyan*, Jia Honglei, Zhuang Jian, Guo Mingzhuo

(College of Biological and Agricultural Engineering, Jilin University, Changchun 130025, China;

Key Laboratory of Bionics Engineering, Ministry of Education, Jilin University, Changchun 130025, China)

Abstract: In the cold areas of Northeast China, maize high-stubble cutting is a novel stalk conservation tillage method, in which the maize stalks are under a unilaterally-fixed no-support cutting status. Thus, reducing the cutting resistance and power consumption of maize stalks under this status is very significant for the development of high-efficiency high-stubble cutting devices. Based on a self-designed testing system that highly restored the maize high-stubble cutting conditions and by means of experimental design and mathematic statistics, the effects of working parameters (blade angle, blade shape, cutting speed and cutting angle) on the maximum cutting resistance and power consumption were studied. By analyzing stress conditions during the stalk cutting process, six mathematic models were built to express the relationships between individual factors and the maximum cutting resistance or cutting power consumption. Through model optimization, the parameter combination for optimal cutting performance of maize stalks under unilaterally-fixed no-support cutting status was obtained: blade angle is 18°, blade shape is isosceles triangle, cutting speed is 9.5 m/s, and cutting angle is 75°. Field validation experiments under this parameter combination showed that the maximum cutting resistance was (55.23±3.50) N (declined by 11.04%), and power consumption was (11.41±1.04) J (declined by 16.65%). The research findings can be a reference for the design and development of maize high-stubble cutting devices.

Keywords: cutting performances, blade angle, working parameters, high-stubble, conservation tillage, mechanism analysis, maize

DOI: 10.3965/j.ijabe.20171001.2589

1 Introduction

The cold areas of Northeast China, which have a low-temperature dry climate, are rich in thick and strong maize stalks[1-3]. The traditional conservation way of

stalk crush covering is restricted by low rotting degree, aggravation of diseases and insects, and reduction of sowing quality[4,5]. Given these restrictions, a novel stalk conservation way－high-stubble cutting, has been popularized in Northeast China[6-10]. Specifically, maize root stubbles are left underground, and 500 mm stalks are left above ground after fall harvest. The root stubbles and stalks are not only effective in alleviating wind corrosion and water corrosion and increasing the soil organic content, but also efficient in preventing diseases and insects compared with the stalk crush covering method[11-13]. During maize high-stubble cutting process, the stalks are cut under the unilaterally-fixed no-support cutting status. The cutting could generate very large cutting resistance and power consumption and increase the working cost, and severely inhibit the popularization of this method.

Thus, the key technical problem in research and development of high-efficiency maize high-stubble cutting devices is how to improve the cutting performance in maize high-stubble works.

Recently, there are a lot of researches about the cutting performances of crop stalks under bilaterally-fixed or supported cutting conditions. A study with an universal testing system show that the cutting speed and cutting angle both significantly affect the cutting resistance under the stalk bilaterally-fixed condition[14-16]. A high-speed camera system revealed that the stalk cutting speed significantly affected the cutting resistance under the bilaterally-fixed condition[11]. The test results with the universal testing system indicated that the blade angle, blade shape and cutting angle all significantly affected the cutting resistance under the supported cutting condition, and a smaller cutting angle was related to a larger cutting resistance[17-19]. Under the supported stalk cutting condition, the cutting power consumption is significantly affected by the cutting speed and declines with the rising cutting speed[20,21]. These studies help to improve the working performance of stalk cutting devices.

However, these studies are focused on the bilaterally-fixed or supported maize stalk cutting condition. In actual works, when the stalks are under other cutting conditions, the significant influence factors and changing laws on cutting performance are all different[22-24]. Therefore, the above studies failed to uncover what factors affect the cutting performance and what are the changing laws during maize high-stubble works. In order to analyze the effects of the parameters of cutter on stalk's cutting performances (the maximum cutting resistance and cutting power consumption), the cutters with different structural parameters (including blade angle, blade shape, cutting speed and cutting angle), were tested on high-stubble conditions of maize with two different cutting conditions (unilaterally-fixed and no-support) using a self-designed testing system by means of experimental design and mathematic statistics. By analyzing the stress conditions of stalks during the cutting process, a mathematic model was built to express the relationships between individual factors and the maximum cutting resistance or cutting power consumption, and these models were used to explain the effects of the factors and the affecting laws. Regression analyses were conducted to build the mathematic models for expressing the relationships between individual factors and the maximum cutting resistance or cutting power consumption. Then the model optimization method was used to find out the parameter combination for optimal cutting performance under unilaterally-fixed no-support status. The research findings will theoretically underlie the development of maize high-stubble cutting devices and promote the maize high-stubble conservation tillage method.

2   Materials and methods

2.1   Materials

The test maize variety of 335, is most commonly-planted in Northeast China. The maize was planted on April 21, 2015. The samples were maize stalks harvested in October 1-7, 2015 at Lishu Town, Changchun, Jinlin Province of China (location: 35.897776ºN, 83.961532ºW). The air humidity was above 60% and air temperature was within 6°C to 14°C during the whole collection course. All samples were packed in plastic wraps immediately after harvest, and then transported to the laboratory is shown in Figure 1. Tests for each sample were conducted within 140 min after harvest. The soils attached to root stubbles and the leaves on the stalks were all reserved. All the tests were conducted at the laboratory of Jilin University in Changchun, China.

Each sample was mainly marked at two positions A and B. During fall high-stubble works, the root stubbles were buried under ground, where position A is the intersection between the stalk and the ground earth, and position B is where a blade cuts the stalk. The stubble height is about 500 mm in actual works. Because all samples were fresh stalks harvested during rainy and wet days, the samples were packed in plastic wrap, and tested within 6 h after harvest for keeping the moisture contents of the samples unchanged basically. Before the cutting

tests, about 20% of the samples were randomly selected for measuring the average moisture content by weighing method with oven-dried at 102°C for 24 h (ASABE Standards, 2006).   The cross sectional area at position B is an ellipse with an average major axis of 26.21 mm and an average minor axis of 22.28 mm.
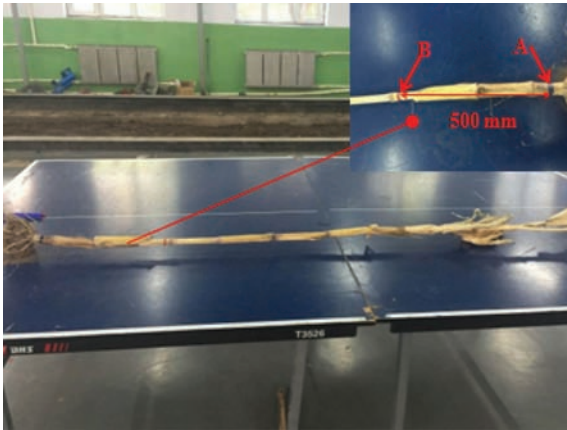

Figure 1   Test samples

2.2   Methods and testing equipment

2.2.1   Selection of testing factors and testing indicators

Given the purposes of this study, four testing factors were selected , including blade angle (15°, 20°, 25° and 30°), blade shape (isosceles triangle and right-angled triangle), cutting speed (4 m/s, 8 m/s, 12 m/s and 16 m/s) and cutting angle (60°, 70°, 80° and 90°), and the maximum cutting resistance and cutting power consumption were chosen as testing indicators.   The cutting angle is defined as the included angle between the stalk axial direction and the cutter radial direction.

Based on the eight combinations of blade angles and blade shapes, sixteen testing cutters were prepared, of which two cutters were made for each combination that one blade was used for cutting test and one blade for examining whether the shape of the test blade was altered.

2.2.2   Design of testing system

The tests were designed to largely reflect the real cutting conditions in terms of both test materials and tool materials.   The testing system mainly consists of a small soil bin, a delivery bed, a numerical control (NC) device, a cutter, a cutting rack, a torque tester, a data acquisition card, Hall sensors, a high-speed camera, and a computer control device (Figure 2).   To guarantee the testing conditions were similar to the real working conditions, the root stubbles were buried in the soil bin.   Under

control by the delivery bed, the stalks were cut at the working speed (8 km/h) of the stubble-typed maize harvester and delivered to the cutting device, which rotated at a constant speed controlled by an NC machine. The cutter's cutting speed v (m/s) was determined jointly from the cutter's rotation speed ω (rad/s) and the stalks' forward speed v_s (m/s).   Specifically, ω was computed as follows:

$$\omega = \frac{\sqrt[2]{v^2 - v_s^2}}{R} \qquad (1)$$

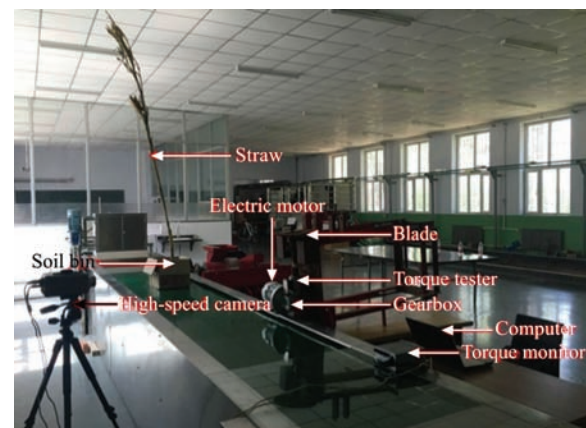where, R is the rotation radius of the cutter, m.

Figure 2   Testing system

As shown in Figure 3, the stalks were buried in the soil bin; area A was at the level of soil surfaces, and area B was 500 mm above the ground surfaces.   The soil bin was fixed onto the delivery bed, whose delivery speed of 8 km/h was set according to the working speed of the stubble-typed maize harvester.   The test cutter was installed on the cutting rack and at a vertical distance of 500 mm from the soil surfaces in the soil bin.   During the tests, the cutting angle was adjusted by changing the rack angle, while the cutting speed was adjusted by changing the rotating speed of the NC machine.   Two Hall sensors were installed at each side of stalk in the soil bin.   When the blade passed through Hall sensor-A, the data acquisition card started timing and reading the data; when it passed through Hall sensor-B, the card stopped timing and reading.   Because the stalks under the unilaterally-fixed no-support cutting status would be bent modestly, the Hall sensor-B should be kept at 20 cm away from the stalks.   Since the stalk cutting is a rapid motion process and in order to accurately observe the deformation changes of stalks under forces, a high-speed

camera with a shooting speed of 0.0001 s was installed into this system and used to observe the deformation status of stalks before being cut, the instantaneous deformation status of stalk epidermis being cut open, and the instantaneous deformation status of stalks after being cut fully open.
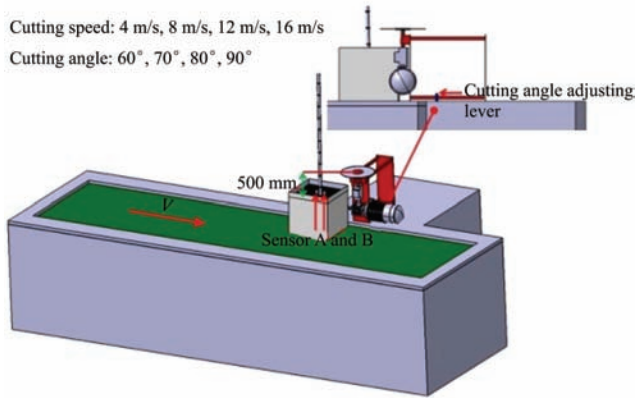

Figure 3   Sketch map of testing system

2.2.3   Abrasion testing of cutting blades during repeated tests

The blades would be abraded somewhat after repeated tests, which would lead to changes in blade shape, blade angle or blade sharpness, thereby reducing the test accuracy.   At the beginning of each test, the test cutter was ground on the grinding wheel, and after that, its blade shape, blade angle and blade sharpness were measured. After each test, the cutter sharpness was assessed again.

Two cutters were made from each combination scheme, one blade used for test and the other one used for contrast to examine whether the shape of the test blade was altered.   The test blade and the contrast blade were connected in head-to-tail to examine whether the blade shapes were different, and thereby to decide whether any blade should be re-processed.

The blade angle was assessed by a Vernier protractor with an accuracy of 2'.   The acceptable error of blade angle is ±0.5°.   The cutters with blade angle beyond this error range would be reground on the grinding wheel. Besides, whether it is any abrasion, distortion and sink need to be examined.

The blade sharpness was assessed by measuring the variation of cutting edge thickness using Scanning Electron Microscopy (SEM).

2.2.4   Detection of maximum cutting resistance

In order to measure the friction-induced torque (T_f)

which caused by the testing system, the NC machine would drive the blade to rotate idly at present speed and cutting angle before each test.   The blade would start to cut stalks and the torque sensor would start to work when the blade's location was above the sensor-A. Simultaneously, the torque data of the stalk cutting and corresponding cutting time were transmitted into the computer.   When the blade rotates to where above the sensor-B, the sensor stops data transmission.   The cutter torque P_t, at cutting time t was computed from the torques P_{it} of five repeated tests.   The P_t was converted to F_t according to Equation (2) by Matlab, and the real pair (F_t, t) would be shown as a point on the cutting resistance – time coordinate system.   Then these points were fitted into a cutting resistance-time curve, from which the cutting resistance changing trend of this blade during stalk cutting was observed.   Figure 4 shows the cutting resistance-time curve $F_{1t}=g_1(t)$ of a blade at blade angle of 15°, cutting speed of 4 m/s, cutting angle of 90° and blade shape of isosceles triangle.   The extremums F_{max} on the cutting resistance-time curve corresponding to each factor combination were determined on Matlab, and were used to compare and analyze the effects of each factor on the maximum cutting resistance.

$$F_t = \frac{\sum_{i=1}^{n_t}(P_{it} - T_f)}{R \cdot n_t} \tag{2}$$

where, F_t is the cutting resistance of a blade at cutting time t, N; P_{it} is the torque measured from the torque sensor at cutting time t in the i-th repeated test, Nm; T_f is the torque due to internal resistance in the testing system, Nm; R is the rotating radius of the cutter, m; n_t is the number of times when P_{it} is larger than T_f at the cutting time t.
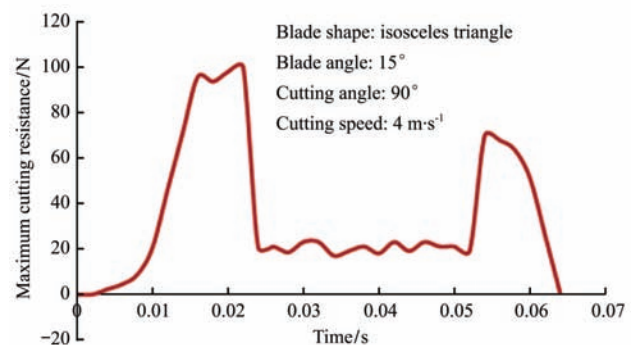

Figure 4   Fitted curve of cutting resistance-time

2.2.5 Determination of cutting power consumption

From Equation (3), the cutting resistance-time curve $F_t = g(t)$ corresponding to each factor combination was converted into a cutting power-time curve $P_t = h(t) = g(t)R\omega$ on Matlab. The area formed by the new curve $P_t = h(t)$ and the time axis is the cutting power consumption W under this factor combination.   Figure 5 shows the $P_t = h(t)$ of a blade at blade angle of 15°, cutting speed of 4 m/s, cutting angle of 90° and blade shape of isosceles triangle.   The W (J) is computed from Equation (4):

$$FP_t = h(t) = g(t)R\omega \tag{3}$$

$$W = \int R\omega g(t)\mathrm{d}t \tag{4}$$

where, P_t is the torque of a blade at the cutting time t, Nm; ω is the preset rotating speed of the blade, rad/s; R is the rotating radius of the blade, m.
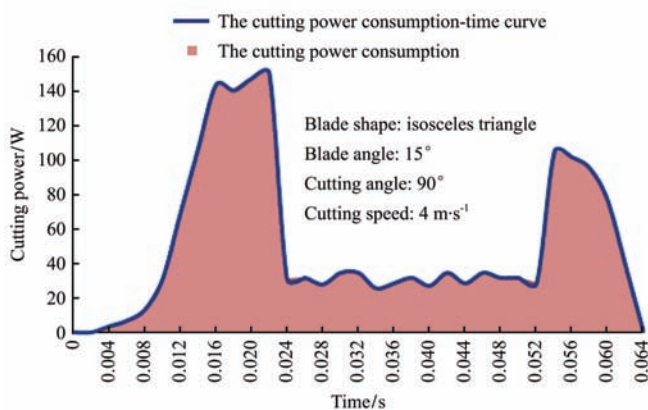

Figure 5   Cutting power-time fitted curve and cutting power consumption

2.2.6 Determination of stalk force status

The stalk forces statuses in the cutting test of each factor combination were recorded by a high-speed camera. The results showed that all stalks undergo the compressed status first and then the compressed and cut status (Figure 6).   As shown in the statuses before being cut open, the epidermis and interior of stalks were both deformed, confirming the occurrence of compressed status.   As shown from the instantaneous status when stalk epidermis was cut open, the stalks were cut into two parts, and the epidermis and interior were both deformed, confirming the coexistence of compressed and cut statuses.   As shown from the instant when the stalk epidermis was fully cut open, the stalks were still deformed, confirming the coexistence of compressed and cut statuses.
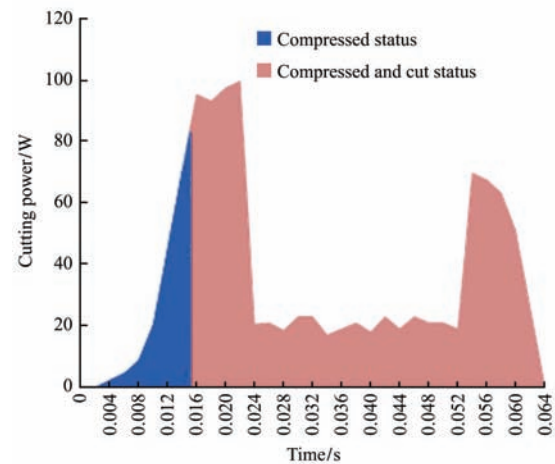

Figure 6   Stalk force statuses

3   Test results and discussion

3.1   Test results

(1) Effects of blade angle on maximum cutting resistance and cutting power consumption

The test data were assessed via analysis of variance (ANOVA) on SPSS.   The histograms of maximum cutting resistance versus blade angle and cutting power consumption versus blade angle are shown in Table 1, respectively.   Clearly, at cutting speed of 4 m/s or 8 m/s, the maximum cutting resistance was significantly affected by the blade angle ($p<0.05$); it continuously declined with the drop of blade angle and the downtrend became gradually gentle (Table 1).   The effect of blade angle on maximum cutting resistance was not significant when the cutting speed exceeded 12 m/s ($p>0.05$).

Moreover, at the cutting speed of 4 m/s or 8 m/s, the cutting power consumption was significantly affected by the blade angle ($p<0.05$); it gradually reduced with the decline of blade angle, and the downtrend became gentle gradually (Table 1).   The effect of blade angle on cutting power consumption was not significant when the cutting speed exceeded 12 m/s ($p>0.05$).

By comparison from Table 1, the results showed that the blade angle and cutting speed imposed an interactive effect on both the maximum cutting resistance and cutting power consumption.

(2) Effects of cutting speed on maximum cutting resistance and cutting power consumption

The test data were assessed via ANOVA on SPSS. The histograms of maximum cutting resistance versus cutting speed and cutting power consumption versus

cutting speed are shown in Table 1, respectively. The maximum cutting resistance was significantly affected by cutting speed ($p<0.05$) and declined with the rise of cutting speed and the downtrend became gradually gentle

(Table 1). The cutting power consumption was significantly affected by the cutting speed ($p<0.05$), and it first dropped and then increased with the rise of cutting speed.

Table 1　Test results of relationships among blade angle, cutting resistance and cutting power consumption

Blade shape	Blade angle /(°)	Cutting angle /(°)	Cutting speed /m·s⁻¹							
			4	8	12	16	4	8	12	16
			Maximum cutting resistance /N				Cutting power consumption /J			
Isosceles triangle	90	15	97.47	86.92	80.66	74.28	15.27	12.58	24.69	32.14
		20	103.11	91.36	82.40	77.71	16.72	14.58	24.37	31.88
		25	110.06	97.54	78.59	74.56	19.23	16.23	24.56	31.59
		30	120.84	106.41	83.17	76.12	23.01	18.59	24.84	32.01
	80	15	77.32	68.58	61.45	55.65	13.42	10.64	22.31	28.99
		20	81.78	72.32	59.74	56.18	15.37	12.61	22.04	29.24
		25	88.52	77.21	64.12	54.71	17.98	14.00	22.57	29.58
		30	98.91	85.27	63.81	56.47	20.47	16.62	22.00	30.03
	70	15	74.41	65.23	56.71	54.71	11.85	9.02	20.71	25.96
		20	79.29	70.48	58.11	53.77	13.92	10.77	21.12	26.05
		25	86.01	74.56	58.17	54.16	16.43	12.43	20.05	26.02
		30	95.17	80.27	57.29	52.39	18.85	15.01	20.56	25.32
	60	15	92.71	81.34	73.21	67.19	13.58	10.81	23.84	29.84
		20	99.62	86.48	71.19	67.72	15.87	12.67	23.09	30.21
		25	105.43	93.02	74.35	69.24	18.02	14.22	23.91	30.02
		30	116.08	102.07	70.98	67.45	20.59	17.28	23.56	30.18
Right-angled triangle	90	15	106.53	96.03	89.88	83.86	17.43	14.39	27.02	33.57
		20	112.78	100.28	90.10	84.05	18.69	16.61	26.89	33.98
		25	121.00	107.53	88.76	83.60	21.31	18.54	26.83	34.13
		30	132.16	117.37	89.45	85.02	25.03	21.00	26.59	34.08
	80	15	85.98	77.12	71.47	65.46	15.68	12.73	24.43	31.92
		20	92.26	81.33	69.53	64.01	17.81	14.59	24.86	31.31
		25	97.17	85.98	72.43	63.79	20.04	16.23	24.08	32.08
		30	109.05	95.48	73.71	65.12	22.87	18.74	24.25	31.16
	70	15	83.56	74.59	64.23	61.33	14.02	11.08	22.67	27.01
		20	90.34	80.32	67.31	62.59	16.13	12.56	22.96	26.74
		25	98.12	86.84	66.32	61.87	18.53	14.52	23.12	26.59
		30	106.02	92.81	64.39	63.89	21.21	16.83	23.08	27.02
	60	15	101.05	90.68	83.45	77.98	15.89	12.72	26.03	34.24
		20	110.31	96.31	85.61	79.20	17.23	14.23	25.51	33.48
		25	120.37	102.07	84.78	79.31	20.29	16.31	25.13	32.89
		30	130.67	113.76	84.45	77.57	23.12	19.58	26.07	33

(3) Effects of cutting angle on maximum cutting resistance and cutting power consumption

The test data were assessed via ANOVA on SPSS. The histograms of maximum cutting resistance versus cutting angle and cutting power consumption versus cutting angle are shown in Table 1, respectively. Both maximum cutting resistance and cutting power consumption were significantly affected by the cutting angle, and both first declined and then increased with the drop of cutting angle (Table 1).

(4) Effects of blade shape on maximum cutting resistance and cutting power consumption

The test data were assessed via ANOVA on SPSS. The histograms of maximum cutting resistance versus blade shape and cutting power consumption versus blade shape are shown in Table 1, respectively. Clearly, the maximum cutting resistance and cutting power consumption were both significantly affected by the blade shape ($p<0.05$), but they were both very small when the shape was an isosceles triangle.

3.2 Discussion

3.2.1 Mathematical models of each factor versus cutting resistance or cutting power consumption

By analyzing the force statuses of stalks and blades during the cutting process, a mathematic model was built to express the relationships between individual factors and the cutting resistance or cutting power consumption, and to discuss how these factors affect the maximum cutting resistance or cutting power consumption. Results showed that during the cutting process, all stalks first enter the compressed status and then the compressed and cut status. Thus, the model between cutting resistance and the blade geometric morphology should be built under the compressed status, and the compressed-cut status.

For any grinding way, the edge blade thickness would never be 0, the blade thickness can be described as dL. As shown in Figure 7a, a blade could be equivalently considered as the connection of countless cross-sections, so the geometric shape of a blade can be equivalently considered as a connection of countless right-angle trapezoids or isosceles trapezoids, while each trapezoid is regarded as a micro-unit of the blade. Based on the same principles, a stalk is subdivided into countless dL-thick micro-units (Figure 7b).

The cutting work at point B of the stalk (500 mm above ground) can be equivalently regarded as the cutting work of countless cutter micro-units on the stalk micro-unit j. The cutting resistance of a cutter on the stalk can be considered as a vector sum of cutting resistances imposed by all blade micro-units on the j-th stalk micro-unit.

Taking the blade micro-unit m and the stalk micro-unit j as objects, as shown in Figure 8a, the force status of the blade micro-unit m at cutting time t consists of pressures N_{mt}, N'_{mt} and N''_{mt} of stalk micro-unit j at three directions, frictions f'_{mt} and f''_{mt} at two directions, and the internal force Q_{mt} imposed from other blade micro-units. The cutting resistance F_{mt} of blade micro-unit m at cutting time t can be deduced as follows:

$$\overrightarrow{F_{mt}} = \overrightarrow{N_{mt}} + \overrightarrow{N'_{mt}} + \overrightarrow{N''_{mt}} + \overrightarrow{f'_{mt}} + \overrightarrow{f''_{mt}} + \overrightarrow{Q_{mt}} \qquad (5)$$

At the cutting time t, the cutting resistance F_t of the cutter is the vector sum of cutting resistances imposed on the cutter micro-units at time t and F_t can be computed as follows:

$$\overrightarrow{F_t} = \sum_m \overrightarrow{F_{mt}} = \sum_m (\overrightarrow{N_{mt}} + \overrightarrow{N'_{mt}} + \overrightarrow{N''_{mt}} + \overrightarrow{f'_{mt}} + \overrightarrow{f''_{mt}} + \overrightarrow{Q_{mt}}) \quad (6)$$

$$\begin{cases} f'_{mt} = N'_{mt} \tan \varphi \\ f''_{mt} = N''_{mt} \tan \varphi \end{cases} \qquad (7)$$

$$\sum_m \overrightarrow{Q_{mt}} = 0 \qquad (8)$$

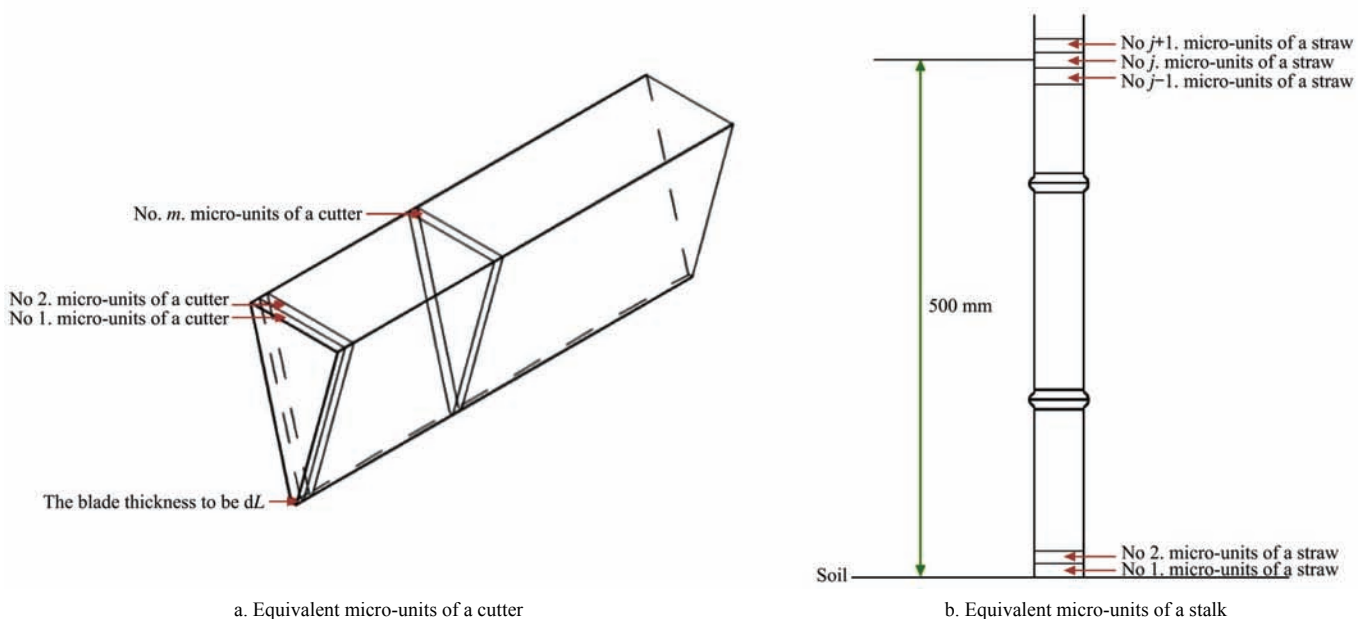where, φ is the friction angle between stalk and cutter, rad.

a. Equivalent micro-units of a cutter

b. Equivalent micro-units of a stalk

Figure 7 Equivalent micro-units of cutter and stalk

a. Force status analysis of blade micro-unit m

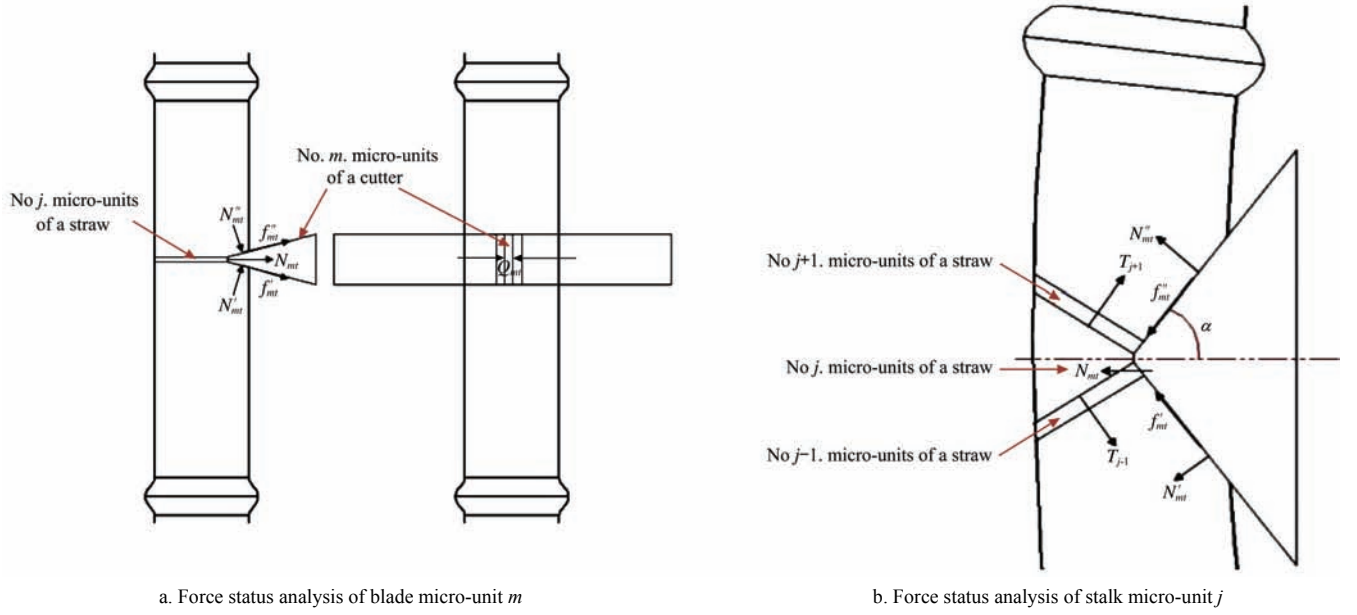b. Force status analysis of stalk micro-unit j

Figure 8   Force status analysis

From Equations (6)-(8), the F_t was calculated by the following equation:

$$F_t = \sum_m (N_{mt} + N'_{mt}\sin\alpha + N'_{mt}\tan\varphi\cos\alpha + N''_{mt}\sin\alpha + N''_{mt}\tan\varphi\cos\alpha) \quad (9)$$

where, α is the half of blade angle, rad.

The force status of stalk micro-unit j (Figure 8b) consists of pull forces T_{j-1} and T_{j+1} from stalk micro-units (j-1) and (j+1), respectively; Pressures N_{mt}, N'_{mt} and N''_{mt} at three directions and the frictions f'_{mt} and f''_{mt} at two directions imposed by all blade micro-units. Thus, the radial force status under the compressed status and the radial force status under the compressed-cut status can be expressed by Equations (10) and (11).

$$\begin{cases} \sum_m (N_{mt} + N'_{mt}\sin\alpha + N'_{mt}\tan\varphi\cos\alpha + N''_{mt}\sin\alpha + \\ N''_{mt}\tan\varphi\cos\alpha) - T_{j-1}\sin\alpha - T_{j+1}\sin\alpha = \int_S G\gamma_j ds \\ \gamma_j < \gamma_{j\max} \end{cases} (10)$$

$$\begin{cases} \sum_m (N_{mt} + N'_{mt}\sin\alpha + N'_{mt}\tan\varphi\cos\alpha + N''_{mt}\sin\alpha + \\ N''_{mt}\tan\varphi\cos\alpha) - T_{j-1}\sin\alpha - T_{j+1}\sin\alpha = \int_S \tau_{j\max} ds \\ \gamma_j = \gamma_{j\max} \end{cases} (11)$$

$$\tau_{j\max} < G\gamma_{j\max} \quad (12)$$

$$T_{j-1} = \sum_{k=1}^{j-1} E\varepsilon_k \quad (13)$$

$$T_{j+1} = \sum_{k=j+1} E\varepsilon_k \quad (14)$$

where, γ_j is the compressed deformation of stalk micro-unit j; $\tau_{j\max}$ is the limit shear force of stalk micro-unit j, Pa; G is the compressed elasticity modulus of stalks; E is the tensile elasticity modulus of stalks; ε_k is the tensile deformation of any stalk micro-unit k.

The model (Equation (15)) which could express the relationship between cutting resistance and blade angle under the compressed status was determined by Equations (10), (12)-(14); The model (Equation (16)) which could express the relationship between cutting resistance and blade angle under the compressed-cut status was determined by Equations (11)-(15).

$$\begin{cases} F_t = \int_{S_j} G\gamma_j ds + \sum_{K=1}^{j-1} E\varepsilon_k\sin\alpha + \sum_{K=j+1} E\varepsilon_k\sin\alpha \\ \gamma_j < \gamma_{j\max} \end{cases} (15)$$

$$\begin{cases} F_t = \int_{S_j} \tau_{j\max} ds + \sum_{K=1}^{j-1} E\varepsilon_k\sin\alpha + \sum_{K=j+1} E\varepsilon_k\sin\alpha \\ \gamma_j = \gamma_{j\max} \end{cases} (16)$$

From Equations (15) and (16), mathematical models expressing the relationship ① between cutting resistance and blade angle was established as Equation (17):

$$\begin{cases} \gamma_j = \gamma_{j\max}: F_t = \int_{S_j} \tau_{j\max} ds + \sum_{K=1}^{j-1} E\varepsilon_k\sin\alpha + \sum_{K=j+1} E\varepsilon_k\sin\alpha \\ \gamma_j < \gamma_{j\max}: F_t = \int_{S_j} G\gamma_j ds + \sum_{K=1}^{j-1} E\varepsilon_k\sin\alpha + \sum_{K=j+1} E\varepsilon_k\sin\alpha \end{cases} (17)$$

From Equations (15) and (16), mathematical models

expressing the relationship ② between cutting power consumption and blade angle was established as Equation (18):

$$W = \int (\int_{S_j} G\gamma_j ds + \sum_{K=1}^{j-1} E\varepsilon_{km} \sin\alpha + \sum_{K=j+1} E\varepsilon_{km} \sin\alpha) dt +$$

$$\int (\int_{S_j} \tau_{j\max} ds + \sum_{K=1}^{j-1} E\varepsilon_{km} \sin\alpha + \sum_{K=j+1} E\varepsilon_{km} \sin\alpha) dt = \sum_{t=0} F_t V dt$$

(18)

3.2.2   Effects of each factor on maximum cutting resistance and cutting power consumption, and analysis of interactive mechanisms

(1) Effects of blade angle or cutting speed on maximum cutting resistance and cutting power consumption, and analysis of interactive mechanisms

To simulate the real in-field working statuses of a stubble-reserved maize harvester, the stalk advancing speed was set at 8 km/h.   From Equations (1) and (2), we know the sliding cutting angle τ_d is enlarged with the rise of cutting speed.

$$\tau_d = \arctan\frac{\omega R}{\sqrt{(\omega R)^2 + v_s^2}}$$

(19)

where, τ_d is the dynamic sliding cutting angle, rad; v_s is the advance speed of stalks, m/s.

When the dynamic sliding cutting angle τ_d is larger than 0, the cutting blade angle of cutter micro-unit m is transferred from the structural blade angle 2α into the real cutting blade angle $2\alpha_d$ (Figure 9), where α_d can be determined from Equation (20).   The model ③ (Equation (21)), which could express the relationship and interaction between the real cutting blade angle and the cutting speed was derived from Equations (19) and (20).

$$\alpha_d = \arctan(\tan\alpha \cos\tau_d)$$

(20)

$$\alpha_d = \arctan\left\{\tan(2\alpha)\cos\left[\arctan\frac{\omega R}{\sqrt{(\omega R)^2 + v_s^2}}\right]\right\}$$

(21)

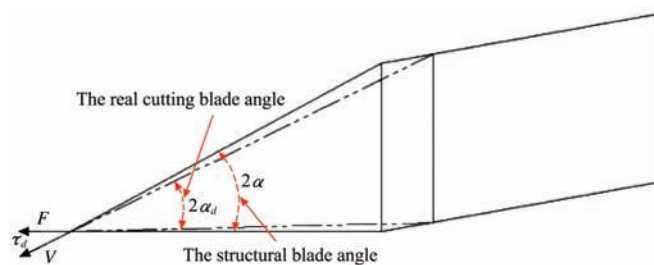where, α_d is the real cutting blade angle, rad.

Figure 9   Schematic diagram of conversion of cutter blade angle

Equation (22) was obtained from models ① and ③. From Equations (1), (21) and (22), the acting laws can be explained as follows: 1) When the cutting speed was very low, the cutting resistance reduced with the decline of blade angle, and the downtrend became gentle gradually; 2) The cutting resistance was enhanced with the rise of cutting speed; 3) When the cutting speed reached a certain level, the real cutting blade angle $2\alpha_d$ reduced rapidly, so for cutters with different structural blade angles 2α, the real cutting edge angles $2\alpha_d$ during cutting process were very similar.   This is because at very small blade angle, the changing trend of cutting resistance was very gentle; so when the cutting speed was above 12 m/s, the effect of blade angle on the cutting resistance was not significant any more.

$$\begin{cases} \dfrac{\partial F_t}{\partial\alpha} > 0 \\ \dfrac{\partial^2 F_t}{\partial\alpha^2} > 0 \\ \dfrac{\partial F_t}{\partial v} > 0 \\ \dfrac{\partial\alpha_d}{\partial v} > 0 \end{cases}$$

(22)

From models ② and ③, The acting laws can be explained as follows: 1) At very low cutting speed, the cutting power consumption is reduced with the decline of blade angle and the downtrend is gradually gentle; 2) When the cutting speed reached a certain level, the real blade angle $2\alpha_d$ rapidly reduced, so for cutters with different structural blade angles 2α, the real blade angles $2\alpha_d$ during cutting process were very similar.   This is because at very small blade angle, the changing trend of cutting power consumption was very gentle; so when the cutting speed was above 12 m/s, the effect of blade angle on the cutting power consumption was not significant any more.

From models ② and ③,   the model ④ (Equation (23)) was obtained to explain the relationship between cutting power consumption and cutting speed.   Equation (24) was got by Equation (23).   From Equation (24), it can be explained why the cutting power consumption first reduced and then increased with the rise of cutting speed.

$$W = \int \left\{ \begin{array}{l} \int_{S_j} G\gamma_j ds + \int_{S_j} \tau_{j\max} ds + (\sum_{K=1}^{j-1} E\varepsilon_k + \sum_{K=j+1} E\varepsilon_k + \sum_{K=1}^{j-1} E\varepsilon_k + \\ \sum_{K=j+1} E\varepsilon_k)\sin\left\{ \arctan\left\{ \tan(2\alpha)\cos\left[\arctan\dfrac{\omega R}{\sqrt{(\omega R)^2 + v_s^2}} \right] \right\} \right\} \end{array} \right\} dt$$

(23)

$$\begin{cases} v < v', \dfrac{\partial w}{\partial v} < 0 \\ v = v', \dfrac{\partial w}{\partial v} = 0 \\ v > v', \dfrac{\partial w}{\partial v} > 0 \end{cases}$$

(24)

where, v' is the cutting speed at the extremum point from Equation (24), m/s.

(2) Effects of blade shape on maximum cutting resistance and cutting power consumption, and analyses of mechanisms

Figure 10 shows the resistances during stalk cutting works from two cutters with blade shape of right-angled triangle and blade angle of 2α, and one cutter with blade shape of isosceles triangle and blade angle of 4α. Combining Figure 10 and Equation (22), the model ⑤ could be obtained in Equation (25) which could express the relationship between cutting resistance and blade shape. From Equation (25), the acting laws of the following factors can be explained: 1) the cutting resistance and 2) the cutting power consumption are both very small when the blade shape is an isosceles triangle.

$$\left. \begin{array}{l} \left. \begin{array}{l} \dfrac{\partial F_t}{\partial \alpha} > 0 \\ \dfrac{\partial^2 F_t}{\partial \alpha^2} > 0 \end{array} \right\} \Rightarrow F_{4\alpha t} > 2F_{2\alpha t} \\ F'_{2\alpha t} + F'_{2\alpha t} > F_{4\alpha t} \end{array} \right\} \Rightarrow F'_{2\alpha t} > F_{2\alpha t}$$

(25)

where, $F'_{2\alpha t}$ is the cutting resistance of a cutter with blade shape of right-angled triangle and blade angle of 2α, N; $F_{2\alpha t}$ is the cutting resistance of a cutter with blade shape of isosceles triangle and blade angle of 2α, N; $F_{4\alpha t}$ is the cutting resistance of a cutter with blade shape of isosceles triangle and blade angle of 4α, N.

(3) Effects of cutting angle on maximum cutting resistance and cutting power consumption, and analyses of mechanisms

During high-stubble cutting works (Figure 11), the stalks after cutting would be bent modestly by an angle β, leading to the increase of cutting angle from θ to $\theta+\beta$.

On this basis, the model ⑥ in Equation (26) which could express the relationship between cutting resistance and cutting angle was obtained. As shown in Figure 12 and Equation (26), the maximum cutting resistance and cutting power consumption both droped first and increased then along with the decline of cutting angle.

$$\begin{cases} \gamma_j = \gamma_{j\max} : F_t = \dfrac{\int_{S_j} \tau_{j\max} ds + \sum_{K=1}^{j-1} E\varepsilon_k \sin\alpha + \sum_{K=j+1} E\varepsilon_k \sin\alpha}{\cos(\beta+\theta)} \\ \gamma_j < \gamma_{j\max} : F_t = \dfrac{\int_{S_j} \tau_{j\max} ds + \sum_{K=1}^{j-1} E\varepsilon_k \sin\alpha + \sum_{K=j+1} E\varepsilon_k \sin\alpha}{\cos(\beta+\theta)} \end{cases}$$
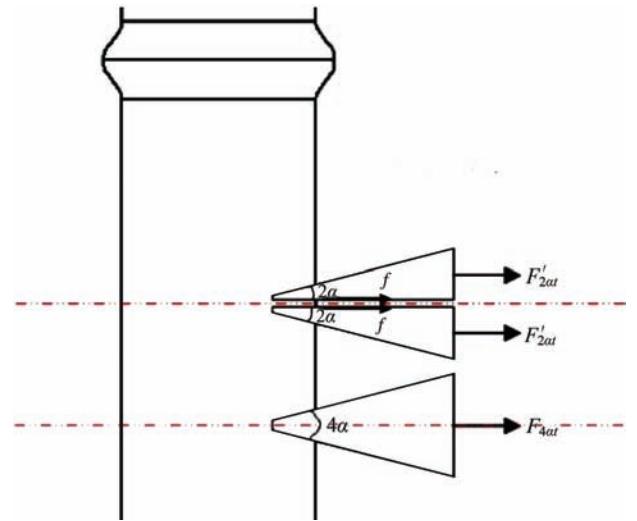
(26)

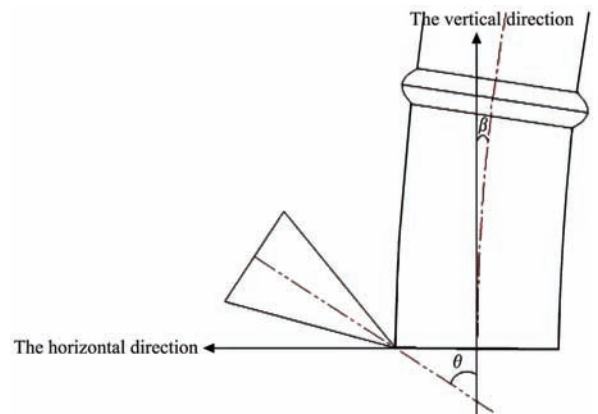Figure 10   Analysis of cutting resistance for cutters with different blade shapes

Figure 11   Analysis of cutting angle changes

3.2.3   Optimal parameter combination and validation

From the above results and the models, it showed that the maximum cutting resistance and cutting power consumption were both significantly affected by blade angle, cutting speed, cutting angle and blade shape

(*p*<0.05), and there was an interaction between blade angle and cutting speed.   This is because the cutting resistance and power consumption are very small when the blade shape is isosceles triangle, so the factor combinations involving this blade shape were selected as data sources, and used to build 3D surface images (Figure

12) on Design-Expert.   With Design-Expert and comprehensively considering low power consumption, low resistance and low cutter wear (blade angle should not be too small), the optimal solution was found: blade shape was isosceles triangle, blade angle was 18°, cutting speed was 9.5 m/s, and cutting angle was 75°.
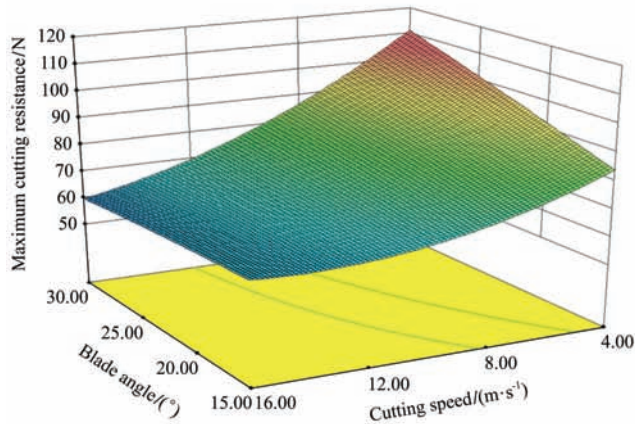
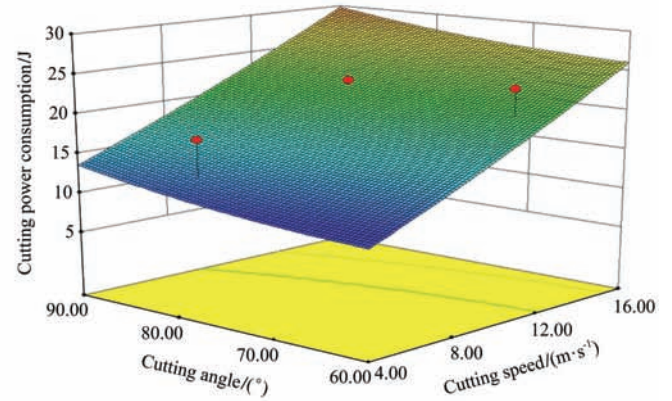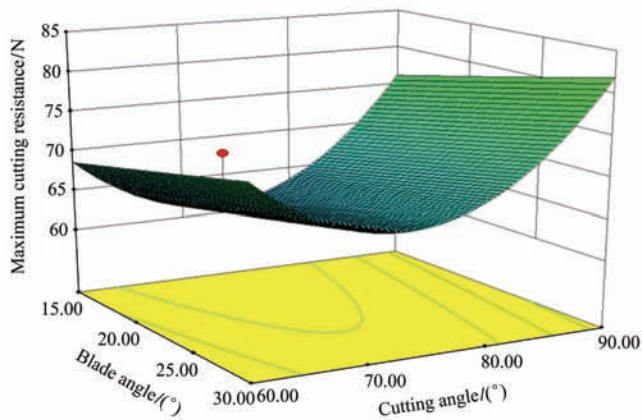a. Maximum cutting resistance versus cutting speed andblade angle
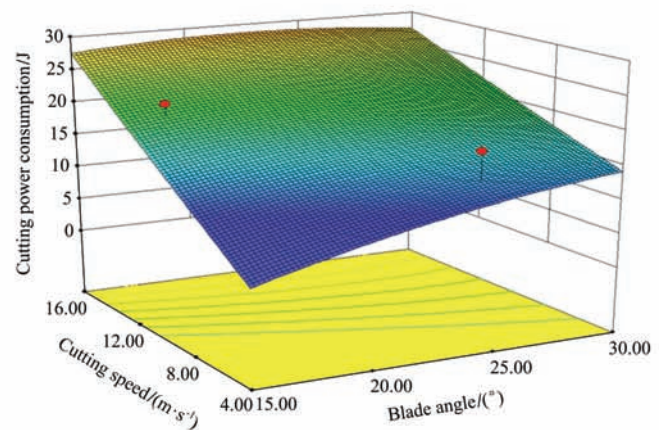
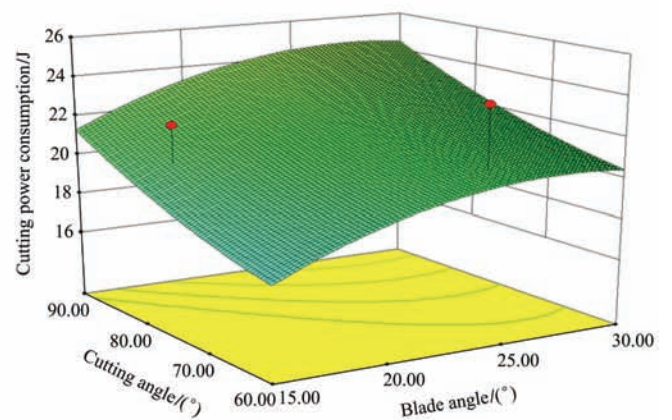b. Cutting power consumption versus cutting speed andblade angle
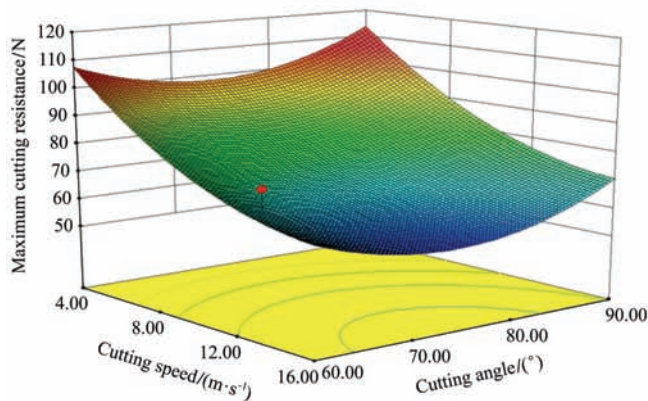
c. Maximum cutting resistance versus cutting speed and cutting angle

d. Cutting power consumption versus cutting speed and cutting angle

e. Maximum cutting resistance versus blade angle and cutting angle

f. Cutting power consumption versus blade angle and cutting angle

Figure 12   Corresponding surface analysis diagram

As shown in Figure 13, one type of commonly-seen high-stubble cutters (saw blade) was selected for validation experiments in field.   Then the cutter edges

were re-processed according to the optimal parameter combination, and the results of maximum cutting resistance and power consumption are shown in Table 2.

Figure 13   Validation experiments in field

Table 2   Maximum cutting resistance and power consumption

Blade	Maximum cutting resistance /N	Cutting power consumption /J
New blade	55.23±3.50	11.41±1.04
Original saw blade	62.08 ±2.41	13.69±1.17

Note: blade angle = 18°, blade shape = isosceles triangle, cutting rate = 9.5 m/s, and cutting angle = 75°

4   Conclusions

1) During high-stubble maize stalks operation, maize stalks will be fixed unilaterally and no-support cutting status. Cutting speed, blade shape and cutting angle have significant influences ($p<0.05$) on the maximum cutting resistance and cutting power consumption. The blade angle has significant influences ($p<0.05$) on the maximum cutting resistance and cutting power consumption if the cutting speed is 4 m/s or 8 m/s, but the blade angle will not have significant influences on the maximum cutting resistance and cutting power consumption any longer if the cutting speed exceeds 12 m/s.

2) Along with the increasing of cutting speed, the maximum cutting resistance decreases gradually (the decreasing tendency becomes gently), the cutting power consumption firstly decreases, and then increases; the maximum cutting resistance and cutting power consumption was relatively low if the blade shape was isosceles triangle. The maximum cutting resistance and cutting power consumption will increase after decreasing along with the decreasing of cutting angle. The maximum cutting resistance and cutting power

consumption will decrease along with the decreasing of blade angle when the cutting speed is 4 m/s or 8 m/s. The reasons for the influenced regulations that mentioned above could be explained by the six mathematical models, which were analysed through stress states of blades and stalks in this paper.

3) According to regression analysis and the consideration of blade life, the best parameters of high-stubble maize stalks are the blade angle is 18°, the blade shape is isosceles triangle, the cutting speed is 9.5 m/s, the cutting angle is 75°. The maximum cutting resistance and cutting power consumption are (55.2± 3.5) N and (28.4±3.2) J respectively under the combined parameters mentioned above. Compared with conventional cutting blade parameter, the maximum cutting resistance and cutting power consumption decreased by 11.04% and 16.65%, respectively. The experimental conclusion and mechanism obtained from this study could provide solid theoretical basis for the design and development of high-stubble maize stalks cutting equipment.

[References]

[1]   Igathinathane C, Womac A R, Sokhansanj S. Corn stalk orientation effect on mechanical cutting. Biosystems Engineering, 2010; 107(2): 97–106.

[2]   Jia H L, Ma C L, Li H Z, Chen Z L. Tillage soil protection of black soil zone in northeast of China based on analysis of conservation tillage in the United States. Transactions of the CSAM, 2010; 41(10): 28–34. (in Chinese)

[3]   Gao H W, Li W Y, Li H W. Conservation tillage technology with Chinese characteristics. Transactions of the CSAM, 2003; 19(3): 1–4. (in Chinese)

[4]   Chattopadhyay P S, Pandey K P. Mechanical properties of sorghum stalk in relation to quasi-static deformation. Journal of Agricultural Engineering Research, 1999; 73(2): 199–206.

[5]   Li Y M, Qin T D, Chen J, Zhao Z. Experiments and

analysis on mechanical property of corn stalk reciprocating cutting. Transactions of the CSAE, 2011; 27(1): 160–164. (in Chinese)

[6] Wu Z Y, Gao H W, Zhang J G. Study on cutting velocity and power requirement in a maize stalk chopping process. Transactions of the CSAM, 2001; 32(2): 38–41. (in Chinese)

[7] Baker J M, Ochsner T E, Venterea R T, Griffisb T. Tillage and soil carbon sequestration-What do we really know? Agriculture, Ecosystems and Environment, 2007; 118(1): 1–5.

[8] Tu J P, Xu X H, Xia Z Y. The study of the cutting-blade and the optimum of the knife-array of field stalk chopper. Journal of Agricultural Mechanization Research, 2003; 2: 102–104. (in Chinese)

[9] Dolan M S, Clappa C E, Allmarasa R R, Bakera J M, Molinab J A E. Soil organic carbon and nitrogen in a Minnesota soil as related to tillage, residue and nitrogen management. Soil and Tillage Research, 2006; 89(2): 221–231.

[10] Yang X M, Drury C F, Reynolds W D, Tan C S. Impacts of long-term and recently imposed tillage practices on the vertical distribution of soil organic carbon. Soil and Tillage Research, 2008; 100(1): 120–124.

[11] Lu C Y, He J, Li H W, Wang Q J, Zhang X C, Liu J A. Finite element analysis and experiment on anti-blocking device based on support cutting. Transactions of the CSAM, 2013; 44: 61–66. (in Chinese)

[12] Lal R, Kimble J M. Conservation tillage for carbon sequestration. Nutrient Cycling in Agroecosystems, 1997; 49(1): 243–253.

[13] West T O, Brandt C C, Wilson B S, Hellwinckel C M, Tyler D D, Marland G, et al. Estimating regional changes in soil carbon with high spatial resolution. Soil Science Society of American Journal, 2008; 72(2): 285–294.

[14] Jam T. Effect of loading rate on mechanical characteristics of wheat and rice stalk. Bulgarian Journal of Agricultural Science, 2013; 19(6): 1452–1458.

[15] Zhao J L, Jia H L, Guo M Z, Jiang, X M, Qu W J, Wang G.

Design and experiment of supported roll-cutting anti-blocking mechanism with for no-till planter. Transactions of the CSAE, 2014; 30(10): 18–28. (in Chinese)

[16] Ma H L, Gao H W, Wei S Y. Driven gap disc cutting mechanism for treating corn stalk and rootstalk. Transactions of the CSAE, 2006; 22(5): 86–89. (in Chinese)

[17] Liao Q X, Gao H W, Shu C X. Present situations and prospects of anti-blocking technology of no-tillage planter. Transactions of the CSAE, 2004; 20(1): 108–120. (in Chinese)

[18] Matin M A, Desbiolles J M A, Fielke J M. Strip-tillage using rotating straight blades: Effect of cutting edge geometry on furrow parameters. Soil and Tillage Research, 2016; 155: 271–279.

[19] Jia H L, Zhao J L, Jiang X M, Guo M Z, Zhuang J, Qi J T, et al. Design and optimization of a double-concave rocker seedmeter for precision seeding. AMA-Agricultural Mechanization in Asia Africa and Latin America, 2015; 46(2): 29–34.

[20] Meng H B, Han L J, Wang J C. Development of the test-bed for testing the mechanical properties of stalk materials. Transactions of the CSAE, 2005; 21(5): 77–80. (in Chinese)

[21] Liu T H, Liang Z H, Guo J D. Experimental comparison of litchi fruit stalk cutting force. Applied Engineering in Agriculture, 2012; 28(2): 297–302.

[22] Liao Q X, Gao H W, Shu C X. Design of sawing anti-blocking mechanism for no-tillage planter and its cutting mechanism. Transactions of the CSAE, 2003; 19(5): 60–70. (in Chinese)

[23] Igathinathane C, Womac A R, Sokhansanj S. Corn stalk orientation effect on mechanical cutting. Biosystems Engineering, 2010; 107(2): 97–106.

[24] Zhang S F, Song Z H, Yan Y F, Li Y D, Li F. Development and experiment of measure and control system for stalk cutting test bench. Transactions of the CSAE, 2013; 29(1): 10–17. (in Chinese)